Arch. Mech., **55**, 3, pp. 275–304, Warszawa 2003

Penny-shaped crack in a piezoceramic cylinder under Mode I loading

F. NARITA, S. LIN, Y. SHINDO

Department of Materials Processing, Graduate School of Engineering, Tohoku University, Aoba-yama 02, Sendai 980-8579, Japan.
e-mail: narita@material.tohoku.ac.jp

THE ELECTROELASTIC response of a penny-shaped crack in a piezoelectric cylinder of finite radius is investigated in this study. Fourier and Hankel transforms are used to reduce the problem to the solution of a pair of dual integral equations. They are then reduced to a Fredholm integral equation of the second kind. Numerical values of the stress intensity factor, energy release rate and energy density factor for piezoelectric ceramics are obtained to show the influence of applied electrical loads.

1. Introduction

MECHANICAL RELIABILITY and durability of piezoelectric ceramics offer important considerations in the design of smart structures and devices. In recent years, significant efforts have been made to the study of fracture behavior of piezoelectric ceramics [1, 2]. In the theoretical studies of the piezoelectric crack problems, the electrical boundary condition imposed across the crack surface remains a debating issue. There are two commonly used electrical boundary conditions. PAK [3] has assumed the crack face to be free of surface charge (the so-called condition of impermeability) while SHINDO *et al.* [4] have assumed that the normal component of the electric displacement and the tangential component of the electric field are continuous across the crack face (the permeable crack boundary condition). The impermeable crack is an inappropriate model [1, 5]. Recently, NARITA and SHINDO [6] obtained a crack growth rate equation of a plane strain slit-like permeable crack parallel to the edges of a narrow piezoelectric ceramic body under Mode I loading. The results indicated that under applied uniform strain, positive electrical fields (electrical fields in poling direction) impede crack propagation while negative electrical fields (electrical fields applied opposite to the poling direction) aid the crack propagation. SHINDO *et al.* [7] also made a finite element analysis (FEA) for the single-edge precracked piezoelectric ceramics for various electric fields to calculate the total potential energy release rate and mechanical strain energy release rate for permeable and impermeable cracks, and performed the

single-edge precracked beam tests on piezoceramics to verify the theoretical predictions of the influence of the applied electric field on the fracture behavior of piezoceramics. They concluded that for applied displacements, the total potential energy release rate and mechanical strain energy release rate for the applied positive electric field under the permeable boundary condition are lower in magnitude than those for the applied negative electric field. This explains an increase in the fracture initiation load in the presence of a positive electric field as observed in the experimental studies. For applied load, the positive (negative) electric field increases (decreases) the total energy release rate and mechanical energy release rate. The FEA results for applied force are in agreement with experimental findings of PARK and SUN [8] and SHINDO *et al.* [9].

The strain energy density theory has opened the door to a new and fruitful area of research in fracture mechanics [10]. In recent works, the energy density criterion was applied to determine the piezoelectric crack growth segments for conditions of positive, negative and zero electric field based on the impermeable assumption. Failure stresses of Mode I and II cracking were also obtained [11]. It is evident that this assumption is valid only for modeling flaws of finite thickness.

This paper considers the electroelastic problem of a penny-shaped crack in a piezoelectric circular cylinder under tensile loading. The method of solution involves the use of Fourier and Hankel transforms to reduce the mixed boundary value problem to a pair of dual integral equations. The solution is then given in terms of a Fredholm integral equation of the second kind. The stress intensity factor, energy release rate and energy density factor are determined and numerical results are shown graphically to demonstrate the influence of applied electric loads.

2. Problem statement and basic equations

Consider a penny-shaped crack of radius a embedded in a long circular piezoelectric cylinder of radius b ($b > a$). It is assumed that the center of the crack is located on the axis of the piezoelectric cylinder and its plane is normal to that axis. Figure 1 shows the geometry of the problem where the position of a point is defined by the cylindrical coordinates (r, θ, z). In this coordinate system, the crack occupies the region $z = 0$, $0 \leq \theta \leq 2\pi$, $0 \leq r < a$. The piezoelectric cylinder is transversely isotropic with hexagonal symmetry; it is subjected to a far-field normal stress $\sigma_{zz} = \sigma_\infty$. Two possible cases of electrical boundary conditions are considered at infinity. The first case is a uniform electric displacement, $D_z = D_\infty$; and the second is a uniform electric field, $E_z = E_\infty$.

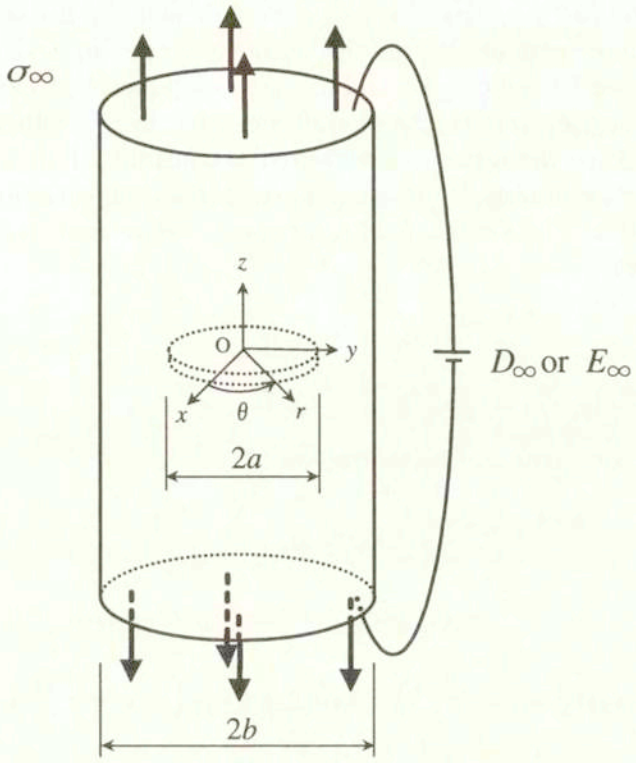

FIG. 1. Geometry and loading of a piezoelectric cylinder with a penny-shaped crack.

The constitutive equations for piezoceramics poled in the z-direction can be written as

$$\left.\begin{aligned} \sigma_{rr} &= c_{11}u_{r,r} + c_{12}\frac{u_r}{r} + c_{13}u_{z,z} - e_{31}E_z \\ \sigma_{\theta\theta} &= c_{12}u_{r,r} + c_{11}\frac{u_r}{r} + c_{13}u_{z,z} - e_{31}E_z \\ \sigma_{zz} &= c_{13}u_{r,r} + c_{13}\frac{u_r}{r} + c_{33}u_{z,z} - e_{33}E_z \\ \sigma_{zr} &= c_{44}(u_{r,z} + u_{z,r}) - e_{15}E_r \end{aligned}\right\} \tag{2.1}$$

$$\left.\begin{aligned} D_r &= e_{15}(u_{r,z} + u_{z,r}) + \epsilon_{11}E_r \\ D_z &= e_{31}\left(u_{r,r} + \frac{u_r}{r}\right) + e_{33}u_{z,z} + \epsilon_{33}E_z \end{aligned}\right\} \tag{2.2}$$

In Eqs. (2.1) and (2.2), $\sigma_{rr}, \sigma_{\theta\theta}, \sigma_{zz}, \sigma_{zr}$ are components of the stress tensor; D_r and D_z the components of electric displacement vector; u_r and u_z the components of displacement vector; E_r and E_z the components of electric field vector; $c_{11}, c_{12}, c_{13}, c_{33}, c_{44}$ the elastic moduli measured in a constant electric field; $\epsilon_{11}, \epsilon_{33}$ the dielectric permittivities measured at constant strain; and e_{15}, e_{31}, e_{33} the piezoelectric constants. A comma implies partial differentiation with respect to the coordinates. The electric field components are related to the electric potential $\phi(r, z)$ by

$$\left.\begin{aligned} E_r &= -\phi_{,r} \\ E_z &= -\phi_{,z} \end{aligned}\right\} \tag{2.3}$$

The governing equations can be written as:

$$\left.\begin{aligned} &c_{11}\left(u_{r,rr} + \frac{u_{r,r}}{r} - \frac{u_r}{r^2}\right) + c_{44}u_{r,zz} \\ &\qquad +(c_{13} + c_{44})u_{z,rz} + (e_{31} + e_{15})\phi_{,rz} = 0 \\ &(c_{13} + c_{44})\left(u_{r,rz} + \frac{u_{r,z}}{r}\right) + c_{33}u_{z,zz} + c_{44}\left(u_{z,rr} + \frac{u_{z,r}}{r}\right) \\ &\qquad +e_{15}\left(\phi_{,rr} + \frac{\phi_{,r}}{r}\right) + e_{33}\phi_{,zz} = 0 \end{aligned}\right\} \tag{2.4}$$

$$(e_{31} + e_{15})\left(u_{r,rz} + \frac{u_{r,z}}{r}\right) + e_{15}\left(u_{z,rr} + \frac{u_{z,r}}{r}\right) + e_{33}u_{z,zz} - \epsilon_{11}\left(\phi_{,rr} + \frac{\phi_{,r}}{r}\right) - \epsilon_{33}\phi_{,zz} = 0. \tag{2.5}$$

In a vacuum, the constitutive equations (2.2) and the governing equations (2.5) become

$$\left.\begin{aligned} D_r &= \epsilon_0 E_r, \\ D_z &= \epsilon_0 E_z; \end{aligned}\right\} \tag{2.6}$$

$$\phi_{,rr} + \frac{\phi_{,r}}{r} + \phi_{,zz} = 0, \tag{2.7}$$

where ϵ_0 is the electric permittivity of the vacuum.

Referring to the semi-infinite region $z \geq 0$, $0 \leq r \leq b$, $0 \leq \theta \leq 2\pi$, the boundary conditions can be expressed in the form

$$\sigma_{zr}(r,0) = 0 \quad (0 \leq r \leq b), \tag{2.8}$$

$$\begin{aligned} \sigma_{zz}(r,0) &= 0 \quad (0 \leq r < a), \\ u_z(r,0) &= 0 \quad (a \leq r \leq b), \end{aligned} \tag{2.9}$$

$$\begin{aligned} E_r(r,0) &= E_r^c(r,0) \quad (0 \leq r < a), \\ \phi(r,0) &= 0 \quad (a \leq r \leq b), \end{aligned} \tag{2.10}$$

$$D_z(r,0) = D_z^c(r,0) \quad (0 \leq r < a), \tag{2.11}$$

$$\sigma_{rr}(b,z) = 0, \tag{2.12}$$

$$\sigma_{rz}(b,z) = 0, \tag{2.13}$$

$$D_r(b,z) = 0, \tag{2.14}$$

$$\text{Case I}: \ \sigma_{zz}(r,z) = \sigma_\infty, \quad D_z(r,z) = D_\infty \quad (0 \leq r \leq b, z \to \infty), \tag{2.15}$$

$$\text{Case II}: \ \sigma_{zz}(r,z) = \sigma_\infty, \quad E_z(r,z) = E_\infty \quad (0 \leq r \leq b, z \to \infty), \tag{2.16}$$

where the superscript c stands for the electric field quantity in the void inside the crack. The far-field normal stress σ_∞ is expressed as

$$\sigma_\infty = \begin{cases} c_1\sigma_0 - e_1 D_\infty & \text{(Case I)}, \\ \sigma_0 - e_2 E_\infty & \text{(Case II)}, \end{cases} \tag{2.17}$$

where

$$c_1 = \frac{(c_{11}+c_{12})\{(c_{11}+c_{12})\bar{c}_{33} - 2(c_{13}^2 + 2c_{13}e_{33}e_{31}/\epsilon_{33} - c_{33}e_{31}^2/\epsilon_{33})\}}{(\bar{c}_{11}+\bar{c}_{12})\{c_{33}(c_{11}+c_{12}) - 2c_{13}^2\}}, \tag{2.18}$$

$$e_1 = \frac{(c_{11}+c_{12})e_{33}/\epsilon_{33} - 2c_{13}e_{31}/\epsilon_{33}}{\bar{c}_{11}+\bar{c}_{12}}, \tag{2.19}$$

$$e_2 = \frac{(c_{11}+c_{12})e_{33} - 2c_{13}e_{31}}{c_{11}+c_{12}}. \tag{2.20}$$

Note that σ_0 is a uniform normal stress for a closed-circuit condition with the potential forced to remain zero (grounded) and $\bar{c}_{11} = c_{11} + e_{31}^2/\epsilon_{33}$, $\bar{c}_{12} = c_{12} + e_{31}^2/\epsilon_{33}$, $\bar{c}_{33} = c_{33} + e_{33}^2/\epsilon_{33}$ are the piezoelectric stiffened elastic constants.

3. Solution procedure

Assume that the solutions u_r, u_z and ϕ are of the form

$$u_r(r,z) = \frac{2}{\pi}\sum_{j=1}^{3}\int_0^\infty [a_j A_j(\alpha)\exp(-\gamma_j\alpha z)J_1(\alpha r) + a_j' B_j(\alpha) I_1(\gamma_j'\alpha r)\cos(\alpha z)]d\alpha + a_\infty r,$$

$$u_z(r,z) = \frac{2}{\pi}\sum_{j=1}^{3}\int_0^\infty \left\{\frac{1}{\gamma_j}A_j(\alpha)\exp(-\gamma_j\alpha z)J_0(\alpha r) + \frac{1}{\gamma_j'}B_j(\alpha)I_0(\gamma_j'\alpha r)\sin(\alpha z)\right\} d\alpha + b_\infty z, \tag{3.1}$$

$$\phi(r,z) = \frac{2}{\pi}\sum_{j=1}^{3}\int_0^\infty \left\{-\frac{b_j}{\gamma_j}A_j(\alpha)\exp(-\gamma_j\alpha z)J_0(\alpha r) + \frac{b_j'}{\gamma_j'}B_j(\alpha)I_0(\gamma_j'\alpha r)\sin(\alpha z)\right\} d\alpha - c_\infty z, \tag{3.2}$$

where $A_j(\alpha)$ and $B_j(\alpha)$ $(j = 1,2,3)$ are the unknowns to be determined, $J_0()$ and $J_1()$ are the zero and first order Bessel functions of the first kind, and $I_0()$ and $I_1()$ are the zero and first order modified Bessel functions of the first kind, respectively. The real constants a_∞, b_∞ and c_∞ will be determined from the far-field loading conditions, and $\gamma_j^2, \gamma_j'^2, a_j, b_j, a_j', b_j'$ $(j = 1,2,3)$ are given in Appendix A. Application of the Fourier transform to Eq. (2.7) yields

$$\phi^c = \frac{2}{\pi}\int_0^\infty C(\alpha)\sinh(\alpha z)J_0(\alpha r)d\alpha \quad (0 \le \gamma < a) \tag{3.3}$$

where $C(\alpha)$ is also unknown. The stresses, electric field intensities and electric displacements can be obtained by making use of Eqs. (2.1)–(2.3), (3.1) and (3.2). The electric field intensities and electric displacements in the void inside the crack can also be obtained from Eqs. (2.3), (2.6) and (3.3).

By applying the far-field loading conditions, the constants a_∞, b_∞ and c_∞ are evaluated as

CASE I.

$$a_\infty = \frac{1}{\delta}\{-(e_{31}e_{33} + c_{13}\epsilon_{33})\sigma_\infty - (c_{13}e_{33} - c_{33}e_{31})D_\infty\},$$

$$b_\infty = \frac{1}{\delta}\Big[\{(c_{11} + c_{12})\epsilon_{33} + 2e_{31}^2\}\sigma_\infty + \{(c_{11} + c_{12})e_{33} - 2c_{13}e_{31}\}D_\infty\Big],$$

(3.4)

$$c_\infty = \frac{1}{\delta}\Big[\{2c_{13}e_{31} - (c_{11} + c_{12})e_{33}\}\sigma_\infty + \{(c_{11} + c_{12})c_{33} - 2c_{13}^2\}D_\infty\Big],$$

$$\delta = (c_{11} + c_{12})(c_{33}\epsilon_{33} + e_{33}^2) + 2(-c_{13}^2\epsilon_{33} + c_{33}e_{31}^2 - 2c_{13}e_{31}e_{33}).$$

CASE II.

$$a_\infty = \frac{1}{2c_{13}^2 - c_{33}(c_{11} + c_{12})}\Big\{c_{13}\sigma_\infty + (c_{13}e_{33} - c_{33}e_{31})E_\infty\Big\},$$

(3.5)

$$b_\infty = \frac{1}{2c_{13}^2 - c_{33}(c_{11} + c_{12})}\Big[-(c_{11} + c_{12})\sigma_\infty + \Big\{2c_{13}e_{31} - (c_{11} + c_{12})e_{33}\Big\}E_\infty\Big],$$

$$c_\infty = E_\infty.$$

The boundary conditions of Eqs. (2.8) and (2.10) lead to the following relations between unknown functions:

$$\frac{f_1}{\gamma_1}A_1(\alpha) + \frac{f_2}{\gamma_2}A_2(\alpha) + \frac{f_3}{\gamma_3}A_3(\alpha) = 0, \tag{3.6}$$

$$\frac{b_1}{\gamma_1}A_1(\alpha) + \frac{b_2}{\gamma_2}A_2(\alpha) + \frac{b_3}{\gamma_3}A_3(\alpha) = 0, \tag{3.7}$$

where

$$f_j = c_{44}(a_j\gamma_j^2 + 1) - e_{15}b_j \qquad (j = 1, 2, 3). \tag{3.8}$$

Application of the mixed boundary conditions in Eqs. (2.9) gives rise to a pair of dual integral equations:

$$\int_0^\infty \alpha F D(\alpha) J_0(\alpha r) d\alpha - \sum_{j=1}^{3} \int_0^\infty \alpha g_j \gamma_j B_j(\alpha) I_0(\gamma_j' \alpha r) d\alpha$$

$$= -\frac{\pi}{2}\sigma_\infty \quad (0 \le r < a), \tag{3.9}$$

$$\int_0^\infty D(\alpha) J_0(\alpha r) d\alpha = 0 \quad (a \le r \le b),$$

where

$$D(\alpha) = \frac{A_1(\alpha)}{d_1} = \frac{A_2(\alpha)}{d_2} = \frac{A_3(\alpha)}{d_3}, \tag{3.10}$$

$$F = \sum_{j=1}^{3} g_j d_j \tag{3.11}$$

$$d_1 = \gamma_1(b_2 f_3 - b_3 f_2), \quad d_2 = \gamma_2(b_3 f_1 - b_1 f_3), \quad d_3 = \gamma_3(b_1 f_2 - b_2 f_1), \tag{3.12}$$

$$g_j = c_{13} a_j - c_{33} + e_{33} b_j \quad (j = 1, 2, 3). \tag{3.13}$$

Through Eqs. (2.12)–(2.14), the unknowns $B_j(\alpha)(j = 1, 2, 3)$ are related to the new parameter $D(\alpha)$ and are given in Appendix B. Note that the only unknown in Eqs. (3.9) is $D(\alpha)$ since $A_j(\alpha), B_j(\alpha)(j = 1, 2, 3)$ are related to $D(\alpha)$ through Eqs. (3.10) and (B.1) in Appendix B.

The solution of a pair of dual integral equations (3.9) may be obtained by using a new function $\Phi(\xi)$ and the result is

$$D(\alpha) = -\frac{\sigma_\infty}{F} a^2 \int_0^1 \Phi(\xi) \sin(a\alpha\xi) d\xi. \tag{3.14}$$

The function $\Phi(\xi)$ is governed by the following Fredholm integral equation of the second kind:

$$\Phi(\xi) + \int_0^1 \Phi(\eta) K(\xi, \eta) d\eta = \xi. \tag{3.15}$$

The kernel function $K(\xi,\eta)$ is

$$K(\xi,\eta)=\frac{4}{\pi^2 F}\sum_{j=1}^{3} g_j\gamma_j^2\int_0^{\infty}\frac{1}{\Delta(\alpha)}\sum_{i=1}^{3} d_i\gamma_i'\{\gamma_i'\alpha M_{ji}(\alpha)K_0(\gamma_i'\alpha b) - N_{ji}(\alpha)K_1(\gamma_i'\alpha b)\}\sinh(\gamma_i' a\alpha\eta)\sinh(\gamma_j' a\alpha\xi)d\alpha \tag{3.16}$$

in which $K_0()$ and $K_1()$ are, respectively, the zero and first order modified Bessel function of the second kind, and $M_{ji}(\alpha)$, $N_{ji}(\alpha)$ $(i,j=1,2,3)$, $\Delta(\alpha)$ are given in Appendix B.

The displacement components u_r, u_z and electric potential ϕ near the crack border are

$$\begin{aligned} u_r &= \frac{k_1\sqrt{r_1}}{F}\sum_{j=1}^{3} a_j d_j\{(\cos^2\theta_1+\gamma_j^2\sin^2\theta_1)^{1/2}+\cos\theta_1\}^{1/2}, \\ u_z &= -\frac{k_1\sqrt{r_1}}{F}\sum_{j=1}^{3}\frac{d_j}{\gamma_j}\{(\cos^2\theta_1+\gamma_j^2\sin^2\theta_1)^{1/2}-\cos\theta_1\}^{1/2}, \end{aligned} \tag{3.17}$$

$$\phi = \frac{k_1\sqrt{r_1}}{F}\sum_{j=1}^{3}\frac{b_j d_j}{\gamma_j}\{(\cos^2\theta_1+\gamma_j^2\sin^2\theta_1)^{1/2}-\cos\theta_1\}^{1/2}, \tag{3.18}$$

and the singular parts of the strains, electric field intensities, stresses and electric displacements in the neighborhood of the crack border are

$$\begin{aligned} \varepsilon_{rr} &= \frac{k_1}{2F\sqrt{r_1}}\sum_{j=1}^{3} a_j d_j R_j^c(\theta_1), \\ \varepsilon_{rz}=\varepsilon_{zr} &= -\frac{k_1}{4F\sqrt{r_1}}\sum_{j=1}^{3}\frac{d_j(a_j\gamma_j^2+1)}{\gamma_j}R_j^s(\theta_1), \\ \varepsilon_{zz} &= -\frac{k_1}{2F\sqrt{r_1}}\sum_{j=1}^{3} d_j R_j^c(\theta_1); \\ E_r &= -\frac{k_1}{2F\sqrt{r_1}}\sum_{j=1}^{3}\frac{b_j d_j}{\gamma_j}R_j^s(\theta_1), \\ E_z &= -\frac{k_1}{2F\sqrt{r_1}}\sum_{j=1}^{3} b_j d_j R_j^c(\theta_1); \end{aligned} \tag{3.19, 3.20}$$

$$\sigma_{rr} = \frac{k_1}{2F\sqrt{r_1}} \sum_{j=1}^{3} m_j d_j R_j^c(\theta_1),$$

$$\sigma_{zz} = \frac{k_1}{2F\sqrt{r_1}} \sum_{j=1}^{3} g_j d_j R_j^c(\theta_1), \tag{3.21}$$

$$\sigma_{zr} = -\frac{k_1}{2F\sqrt{r_1}} \sum_{j=1}^{3} \frac{f_j d_j}{\gamma_j} R_j^s(\theta_1);$$

$$D_r = -\frac{k_1}{2F\sqrt{r_1}} \sum_{j=1}^{3} \frac{n_j d_j}{\gamma_j} R_j^s(\theta_1),$$

$$D_z = \frac{k_1}{2F\sqrt{r_1}} \sum_{j=1}^{3} h_j d_j R_j^c(\theta_1), \tag{3.22}$$

where

$$h_j = e_{31} a_j - e_{33} - \epsilon_{33} b_j, \tag{3.23}$$

$$R_j^c(\theta_1) = \left\{ \frac{(\cos^2\theta_1 + \gamma_j^2 \sin^2\theta_1)^{1/2} + \cos\theta_1}{\cos^2\theta_1 + \gamma_j^2 \sin^2\theta_1} \right\}^{1/2},$$

$$R_j^s(\theta_1) = -\left\{ \frac{(\cos^2\theta_1 + \gamma_j^2 \sin^2\theta_1)^{1/2} - \cos\theta_1}{\cos^2\theta_1 + \gamma_j^2 \sin^2\theta_1} \right\}^{1/2} \tag{3.24}$$

and the polar coordinates r_1 and θ_1 are defined as

$$r_1 = \{(r-a)^2 + z^2\}^{1/2}, \tag{3.25}$$

$$\theta_1 = \arctan\left(\frac{z}{r-a}\right). \tag{3.26}$$

The stress intensity factor k_1 for the permeable crack is obtained as

$$k_1 = \lim_{r \to a^+} \left\{2(r-a)\right\}^{1/2} \sigma_{zz}(r,0) = \frac{2}{\pi} \sigma_\infty \sqrt{a} \Phi(1). \tag{3.27}$$

The electric displacement intensity factor k_D is also given by

$$k_D = \lim_{r \to a^+} \left\{ 2(r-a) \right\}^{1/2} D_z(r,0) = \left(\frac{1}{F} \sum_{j=1}^{3} h_j d_j \right) k_1. \tag{3.28}$$

The stress and electric displacement intensity factors for the impermeable crack are discussed in Appendix C.

By using the concept of crack closure energy and the asymptotic behavior of stresses, displacements, electric displacement and electric potential near the crack border, the total potential energy release rate G may be expressed as

$$G = \lim_{\Delta a \to 0} \frac{1}{\Delta a} \int_0^{\Delta a} \{ \sigma_{zz}(r_1) u_z(\Delta a - r_1) + \sigma_{zr}(r_1) u_r(\Delta a - r_1) + D_z(r_1) \phi(\Delta a - r_1) \} dr_1, \tag{3.29}$$

where Δa is the assumed crack extension. Expression relating G for the permeable crack to k_1 is obtained by substituting representations for the stresses, displacements, electric displacement and electric potential in the vicinity of the crack into Eq. (3.29) and taking the limit. The result is

$$G = -\frac{\pi}{2F^2} \left(F \sum_{j=1}^{3} \frac{d_j}{\gamma_j} - \sum_{j=1}^{3} h_j d_j \sum_{j=1}^{3} \frac{b_j d_j}{\gamma_j} \right) k_1^2. \tag{3.30}$$

The mechanical strain energy release rate G_M includes only the mechanical energy released as the crack extends and is given by

$$G_M = \lim_{\Delta a \to 0} \frac{1}{\Delta a} \int_0^{\Delta a} \left\{ \sigma_{zz}(r_1) u_z(\Delta a - r_1) + \sigma_{zr}(r_1) u_r(\Delta a - r_1) \right\} dr_1. \tag{3.31}$$

Writing the mechanical strain energy release rate expression for the permeable crack in terms of the stress intensity factor, we obtain:

$$G_M = -\left(\frac{\pi}{2F} \sum_{j=1}^{3} \frac{d_j}{\gamma_j} \right) k_1^2. \tag{3.32}$$

The total potential and mechanical strain energy release rates for the impermeable crack are also given in Appendix C.

When the stress intensity factor k_1 and the electric displacement intensity factor k_D are present along the crack border, the fracture criterion should depend

on a combination of k_1 and k_D reaching a critical value. Such a criterion can be developed by referring to the amount of energy stored in a volume element ahead of the crack. The critical value of this energy density will be used to determine whether the piezoceramic has reached the state of failure or not [10, 11]. For the piezoceramic, the energy stored in the volume element dV is

$$dW = \left\{\frac{1}{2}(\sigma_{rr}\varepsilon_{rr} + \sigma_{zr}\varepsilon_{zr} + \sigma_{rz}\varepsilon_{rz} + \sigma_{zz}\varepsilon_{zz}) + \frac{1}{2}(D_r E_r + D_z E_z)\right\} dV. \tag{3.33}$$

Substituting Eqs. (3.19)–(3.22) into Eq. (3.33) yields the quadratic form for the energy density function

$$\frac{dW}{dV} = \frac{1}{r_1}(a_M + a_E)k_1^2 = \frac{S}{r_1} \tag{3.34}$$

in which the coefficients a_M and a_E depend on the angle θ_1 and they are given by

$$a_M = \frac{1}{8F^2}\left\{\sum_{j=1}^{3} m_j d_j R_j^c(\theta_1) \sum_{j=1}^{3} a_j d_j R_j^c(\theta_1) + \sum_{j=1}^{3} \frac{f_j d_j}{\gamma_j} R_j^s(\theta_1) \sum_{j=1}^{3} \frac{d_j(a_j\gamma_j^2 + 1)}{\gamma_j} R_j^s(\theta_1) - \sum_{j=1}^{3} g_j d_j R_j^c(\theta_1) \sum_{j=1}^{3} d_j R_j^c(\theta_1)\right\}, \tag{3.35}$$

$$a_E = \frac{1}{8F^2}\left\{\sum_{j=1}^{3} \frac{n_j d_j}{\gamma_j} R_j^s(\theta_1) \sum_{j=1}^{3} \frac{b_j d_j}{\gamma_j} R_j^s(\theta_1) - \sum_{j=1}^{3} h_j d_j R_j^c(\theta_1) \sum_{j=1}^{3} b_j d_j R_j^c(\theta_1)\right\}. \tag{3.36}$$

The magnitude, S, of the $1/r_1$ energy field in Eq. (3.34) will be referred to as the energy density factor for the permeable crack. The energy density factor for the impermeable crack is also given in Appendix C.

For a penny-shaped crack under tensile loading, fracture will always occur in the normal plane. SIH [10] has assumed that crack initiation starts in a radial direction along which the energy density is a minimum. Necessary and sufficient conditions for S to have a minimum value are

$$\frac{dS}{d\theta_1} = 0, \quad \frac{d^2S}{d\theta_1^2} > 0. \tag{3.37}$$

Rapid crack growth occurs when the minimum energy density factor reaches a critical value:

$$S_{min} = S_c = r_{1c}\left(\frac{dW}{dV}\right)_c, \tag{3.38}$$

where r_{1c} represents the last ligament of slow crack growth, just prior to the onset of rapid fracture. Each increment of stable crack growth $r_{11}, r_{12}, ..., r_{1j}, ..., r_{1c}$ up to the rapid crack propagation is determined by the condition

$$\left(\frac{dW}{dV}\right)_c = \frac{S_1}{r_{11}} = \frac{S_2}{r_{12}} = \cdots = \frac{S_j}{r_{1j}} = \cdots = \frac{S_c}{r_{1c}}. \tag{3.39}$$

If the fracture process due to increasing electromechanical load is unstable, then each increment of crack growth will increase monotonically, i.e.

$$r_{11} < r_{12} < \cdots < r_{1j} < \cdots < r_{1c}. \tag{3.40}$$

The corresponding energy density factors will also increase according to $S_j/r_{1j} = \text{const}$:

$$S_1 < S_2 < \cdots < S_j < \cdots < S_c. \tag{3.41}$$

A stable fracture process corresponds to decreasing increments of the crack growth:

$$r_{11} > r_{12} > \cdots > r_{1j} > \cdots > r_{1a}, \tag{3.42}$$

where r_{1a} is the last increment of growth before the crack arrest. A corresponding decrease in the energy density factors takes place:

$$S_1 > S_2 > \cdots > S_j > \cdots > S_a. \tag{3.43}$$

In the piezoceramic, a combination of the conditions described by Eqs. (3.40) and (3.42) can exist. That is, the increments of crack growth may either increase or decrease, depending on the material properties and the nature of combined electromechanical loading.

4. Numerical results and discussion

The determination of the stress intensity factor, energy release rate and energy density factor for the permeable crack requires the solution of the function $\Phi(\xi)$. The solution of the Fredholm integral equation of the second kind (3.15)

governing $\Phi(\xi)$ has been computed numerically by the use of Gaussian quadrature formulas. Once this is done, k_1, G and S can be found from Eqs. (3.27), (3.30), (3.31) and (3.34). The simultaneous Fredholm integral equations of the second kind (C.11) were also solved numerically to yield the values of the functions $\Phi_1(1)$ and $\Phi_2(1)$. These values were then inserted into Eqs. (C.13) and (C.14) to determine the stress and electric displacement intensity factors for the impermeable crack. The energy release rate and energy density factor were calculated by using Eqs. (C.15), (C.16) and (C.18)–(C.20). The piezoelectric materials are assumed to be the commercially available piezoceramic P-7. The elastic, piezoelectric and dielectric properties of material are listed in Table 1.

Table 1. Material properties of a piezoelectric ceramic P-7.

	Elastic stiffnesses ($\times 10^{10}$N/m^2)					Piezoelectric coefficients (C/m^2)			Dielectric constants ($\times 10^{-10}$C/Vm)	
	c_{11}	c_{33}	c_{44}	c_{12}	c_{13}	e_{31}	e_{33}	e_{15}	ϵ_{11}	ϵ_{33}
P-7	13.0	11.9	2.5	8.3	8.3	−10.3	14.7	13.5	171	186

Figure 2 shows the normalized stress intensity factor $\pi k_1/2\sigma_0 a^{1/2}$ as a function of the crack-radius to cylinder-radius ratio a/b for different values of the normalized electric displacement $e_1 D_\infty/c_1\sigma_0$ (Case I) and for the permeable (exact) and impermeable (approximate) cracks. The data are normalized by the stress intensity factor $2\sigma_0 a^{1/2}/\pi$ of an infinite P-7 piezoelectric ceramic for $D_\infty = 0$ C/m^2 corresponding to the applied uniform displacement. A similar phenomenon was observed for the stress intensity factor of the permeable and impermeable cracks. Note that an increase of a/b causes an increase in the stress intensity factor. When electric displacement is applied, which is equivalent to applying a surface charge, $\pi k_1/2\sigma_0 a^{1/2}$ increases or decreases depending on the direction of the electric displacement. The stress intensity factor k_1 normalized by $2\sigma_\infty a^{1/2}/\pi$ corresponding to the applied uniform stress for the permeable and impermeable crack models is independent of the normalized electric displacement $e_1 D_\infty/c_1\sigma_\infty$. A similar explanation applies to the results shown in Fig. 3 for Case II as the normalized electric field $e_2 E_\infty/\sigma_0$ is varied. In the case of electric field loading, which can be more readily achieved in the laboratory by applying a constant potential difference across the piezoceramic cylinder, applying the field in the positive direction decreases the stress intensity factor, whereas the negative electric field increases it. For $e_1 D_\infty/c_1\sigma_0 \to 1.0$ or $e_2 E_\infty/\sigma_0 \to 1.0$, $\pi k_1/2\sigma_0 a^{1/2}$ approaches zero. The stress intensity factor is also studied for different conditions of the electric potential at infinity of the piezoceramic cylinder:

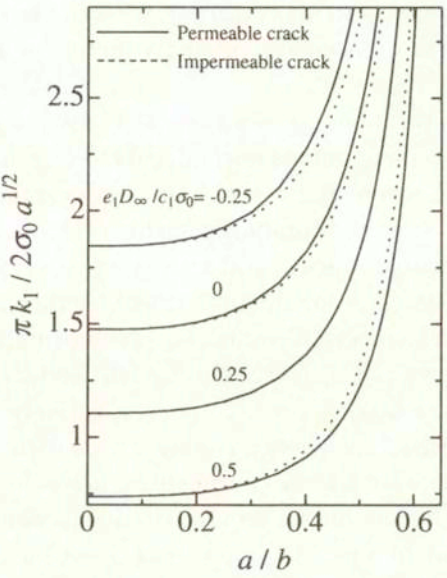

FIG. 2. Stress intensity factor versus a/b for different electric displacement $e_1 D_\infty / c_1 \sigma_0$ (Case I).

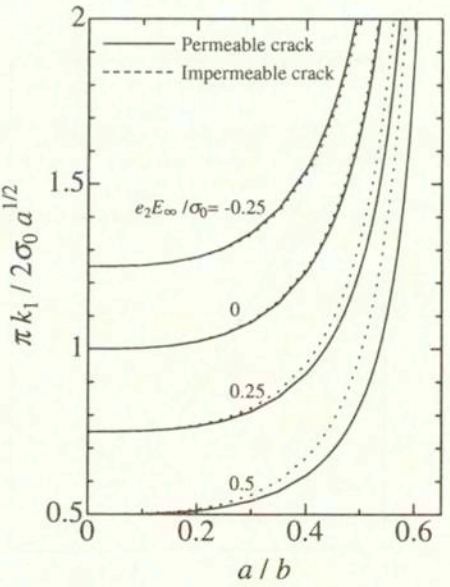

FIG. 3. Stress intensity factor versus a/b for different electric field $e_2 E_\infty / \sigma_0$ (Case II).

an open-circuit condition where the electric potential remains free (zero electric displacements) and a closed-circuit condition with the potential forced to remain zero (grounded). Note that the stress intensity factor for $E_\infty = 0$ is smaller than the one for $D_\infty = 0$.

Figure 4 shows the total energy release rate G for the permeable crack under applied uniform displacement versus normalized electric displacement $e_1 D_\infty / c_1 \sigma_0$ (Case I) for $a/b = 0.5$, where the result has been normalized by the energy release rate G_{D0} for $D_\infty = 0$. For comparison, the mechanical strain energy release rate G_M for the permeable crack, total energy release rate G_I and mechanical strain energy release rate G_{MI} for the impermeable crack are also included in the figure. Energy release rates G_M, G_I and G_{MI} are normalized by the mechanical strain energy release rate G_{MD0}, total energy release rate G_{ID0} and mechanical strain energy release rate G_{MID0} for $D_\infty = 0$, respectively. Comparing the results from the total and mechanical energy release rates, little difference is observed. The total energy release rate for the permeable crack is lower for positive electric displacements and higher for negative electric displacements. Hence, a positive electrical load will tend to slow the crack growth and a negative electrical load will tend to enhance the crack growth. The numerical results for the permeable crack are found to be in excellent agreement with the observations of SHINDO *et al.* [7]. On the other hand, when a positive electrical load is larger, a negative total energy release rate is produced for the impermeable crack. The impermeable assumption leads to an overly attractive prediction regarding the crack

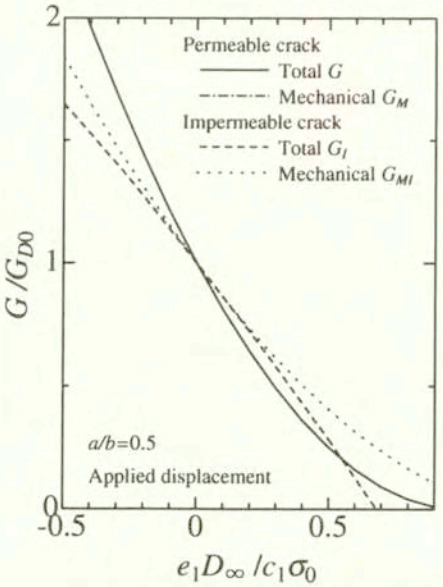

FIG. 4. Energy release rate versus electric displacement $e_1 D_\infty / c_1 \sigma_0$ (Case I).

arresting ability of electrical loads in cracked piezoceramics. Figure 5 shows the corresponding result for Case II. Here the data G, G_M, G_I and G_{MI} have been normalized by the energy release rates G_{E0}, G_{ME0}, G_{IE0} and G_{MIE0} for $E_\infty = 0$, respectively. The presentation of data for the impermeable crack causes confusion in using the electrical boundary conditions on the crack face. Figure 6 gives the plot of the normalized total energy release rate G_I/G_{ID0} for the permeable and impermeable cracks under applied uniform stress versus normalized electric displacement $e_1 D_\infty/c_1\sigma_\infty$ (Case I) for $a/b = 0.5$. Also shown is the normalized mechanical energy release rate G_{IM}/G_{IMD0}.

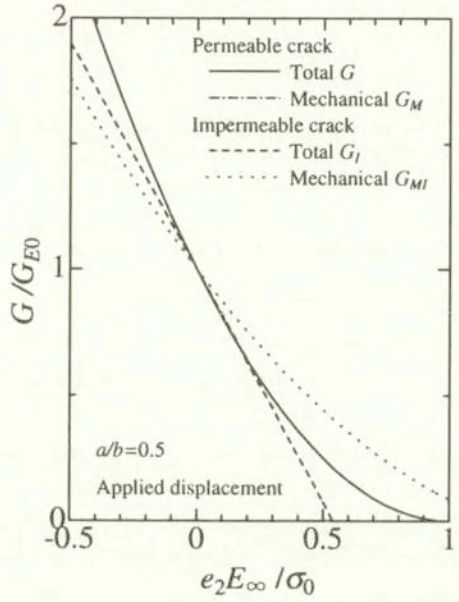

FIG. 5. Energy release rate versus electric field $e_2 E_\infty/\sigma_0$ (Case II).

Figure 7 shows the corresponding result for Case II. Appling the electrical load in either direction decreases the total energy release rate for the impermeable crack and eventually arrests the crack growth. However, experimental investigation does not confirm this crack-arresting behavior. The total and mechanical energy release rates for the permeable crack are independent of the electrical loading.

Figure 8 gives the variation of the normalized energy density factor $\pi^2 S/4a\sigma_0^2$ with angle θ_1 for different values of $e_1 D_\infty/c_1\sigma_0$ (Case I) and $a/b = 0.5$. Excluding the extreme values at the crack boundaries, all curves for the permeable and impermeable cracks possess minimum at $\theta_1 = 0$. The variation of $\pi^2 S/4a\sigma_0^2$ with

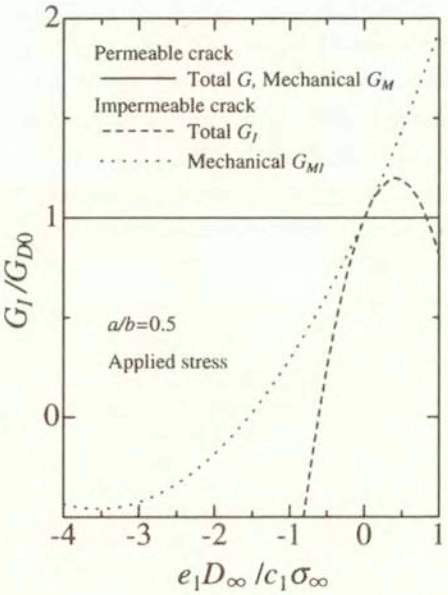

FIG. 6. Energy release rate versus electric displacement $e_1 D_\infty / c_1 \sigma_0$ (Case I).

θ_1 for Case II is found to be similar to that for Case I. Figure 9 shows the crack growth segment r_{1j} (energy density factor S_j) for the permeable crack under applied uniform displacement versus normalized electric displacement $e_1 D_\infty / c_1 \sigma_0$ (Case I) for $a/b = 0.5$ and $\theta_1 = 0$, where r_{1j} (S_j) has been normalized by the crack growth segment r_{1D0} (energy density factor S_{D0}) for $D_\infty = 0$. Also shown are data for the impermeable crack normalized by r_{1ID0} (S_{ID0}) that corresponds to the crack growth segment (energy density factor) for $D_\infty = 0$. The presence of positive electric displacement D_∞ leads to a decrease in the crack growth segment (energy density factor) for the permeable crack. In contrast, the crack growth segment (energy density factor) increases as the electric displacement D_∞ increases in the negative direction. Figure 10 shows the corresponding result for Case II. The data r_{1j} (S_j) and r_{1jI} (S_{jI}) have been normalized due to r_{1E0} (S_{E0}) and r_{1IE0} (S_{IE0}) for $E_\infty = 0$, respectively. For the permeable boundary condition, no difference in the effects of the electrical loads on crack propagation is found for the criteria (the stress intensity factor, total energy release rate, mechanical strain energy release rate and energy density factor). Figures 11 and 12 exhibit the dependence of the crack growth segment (energy density factor) for the permeable and impermeable cracks under applied uniform stress on $e_1 D_\infty / c_1 \sigma_\infty$ and $e_2 E_\infty / \sigma_\infty$, respectively. Based on the energy density criterion for the impermeable crack, we cannot explain the experimental results.

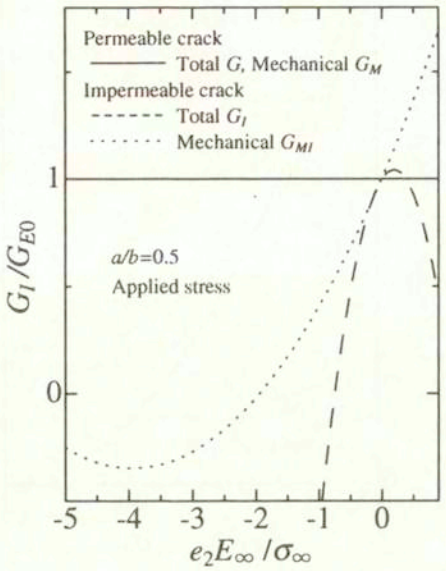

FIG. 7. Energy release rate versus electric field e_2E_∞/σ_0 (Case II).

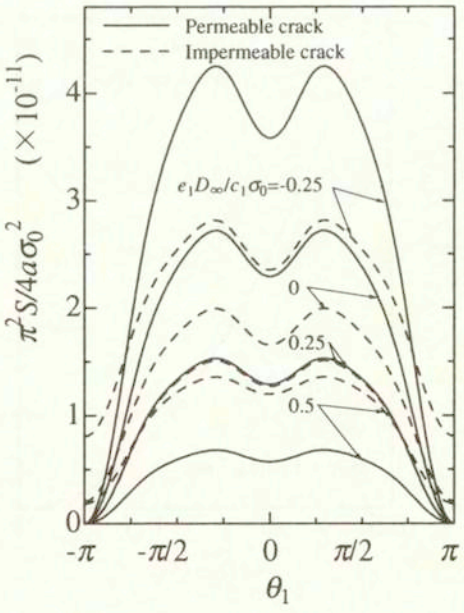

FIG. 8. Energy density factor versus angle θ_1 for a/b=0.5 (Case I).

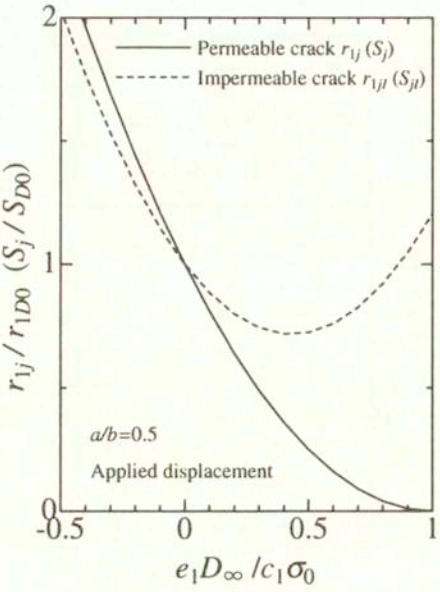

FIG. 9. Crack growth segment (energy density factor) versus electric displacement $e_1D_\infty/c_1\sigma_0$ (Case I).

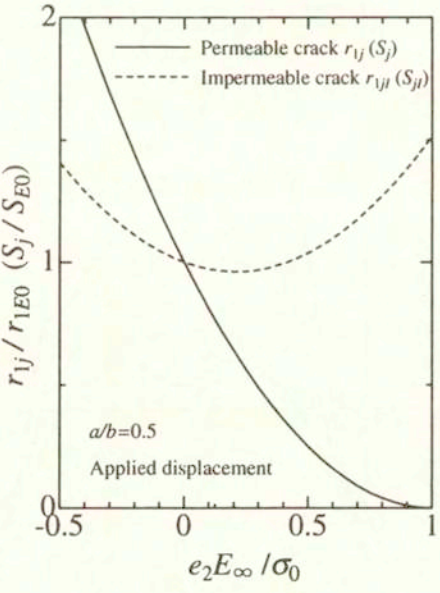

FIG. 10. Crack growth segment (energy density factor) versus electric field e_2E_∞/σ_0 (Case II).

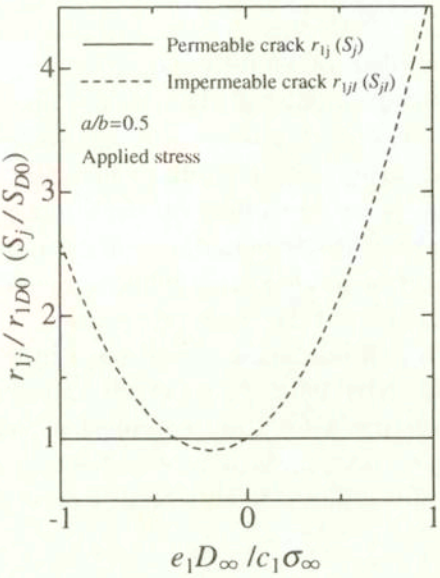

FIG. 11. Crack growth segment (energy density factor) versus electric displacement $e_1 D_\infty / c_1 \sigma_\infty$ (CaseI).

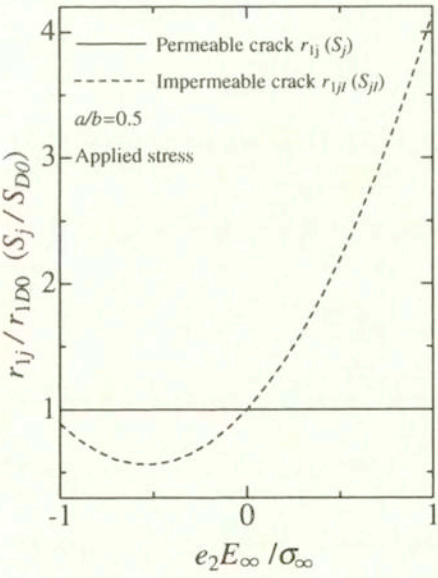

FIG. 12. Crack growth segment (energy density factor) versus electric field $e_2 E_\infty / \sigma_\infty$ (Case II).

5. Conclusions

The electroelastic problem of a piezoceramic cylinder with a penny-shaped crack has been theoretically analyzed. The results are expressed in terms of the stress intensity factor, energy release rate and energy density factor. It is found that the stress intensity factor tends to increase with increasing crack-radius to cylinder-radius ratio, depending on the electrical boundary condition on the crack face. For the permeable boundary condition, positive electrical loads impede crack propagation in piezoelectric cylinder under applied displacement while negative electrical loads aid the crack propagation. The experimental study has shown that crack growth inhibition corresponds to a positive field. For applied stress, electric fields have no effect on crack propagation. No consensus is reached on the fracture criteria for the impermeable piezoelectric cracks, and the stress intensity factor, energy release rate and energy density factor criteria for the permeable crack are superior to the fracture criteria for the impermeable crack.

Acknowledgement

The work was supported by the Grant-in-Aid for Encouragement of Young Scientists from the Ministry of Education, Culture, Sports, Science and Technology of Japan

Appendix A

γ_j^2 $(j = 1, 2, 3)$ in Eqs. (3.1), (3.2) are the roots of the following characteristic equation:

$$a_0\gamma^6 + b_0\gamma^4 + c_0\gamma^2 + d_0 = 0, \tag{A.1}$$

where

$$\begin{aligned}
a_0 &= c_{44}(c_{33}\epsilon_{33} + e_{33}^2),\\
b_0 &= -2c_{44}e_{15}e_{33} - c_{11}e_{33}^2 - c_{33}(c_{44}\epsilon_{11} + c_{11}\epsilon_{33}) + \epsilon_{33}(c_{13} + c_{44})^2\\
&\quad + 2e_{33}(c_{13} + c_{44})(e_{31} + e_{15}) - c_{44}^2\epsilon_{33} - c_{33}(e_{31} + e_{15})^2,\\
c_0 &= 2c_{11}e_{15}e_{33} + c_{44}e_{15}^2 + c_{11}(c_{33}\epsilon_{11} + c_{44}\epsilon_{33}) - \epsilon_{11}(c_{13} + c_{44})^2\\
&\quad - 2e_{15}(c_{13} + c_{44})(e_{31} + e_{15}) + c_{44}^2\epsilon_{11} + c_{44}(e_{31} + e_{15})^2,\\
d_0 &= -c_{11}(c_{44}\epsilon_{11} + e_{15}^2)
\end{aligned} \tag{A.2}$$

and, $\gamma_j'^2$, a_j, b_j, a_j', b_j' $(j = 1, 2, 3)$ stand for the abbreviations:

$$\gamma_j'^2 = \frac{1}{\gamma_j^2}, \tag{A.3}$$

$$a_j = \frac{(e_{31} + e_{15})(c_{33}\gamma_j^2 - c_{44}) - (c_{13} + c_{44})(e_{33}\gamma_j^2 - e_{15})}{(c_{44}\gamma_j^2 - c_{11})(e_{33}\gamma_j^2 - e_{15}) + (c_{13} + c_{44})(e_{31} + e_{15})\gamma_j^2}, \tag{A.4}$$

$$b_j = \frac{(c_{44}\gamma_j^2 - c_{11})a_j + (c_{13} + c_{44})}{e_{31} + e_{15}}, \tag{A.5}$$

$$a_j' = -a_j\gamma_j^2, \tag{A.6}$$

$$b_j' = -b_j. \tag{A.7}$$

Appendix B

The unknowns $B_j(\alpha)(j = 1, 2, 3)$ can be related to the new parameter as

$$B_1(\alpha) = \frac{1}{\Delta(\alpha)} \sum_{i=1}^{3} d_i \int_0^\infty \{M_{1i}(\alpha)G_i(s, \alpha) + N_{1i}(\alpha)G_i'(s, \alpha), \}D(s)ds,$$

$$B_2(\alpha) = \frac{1}{\Delta(\alpha)} \sum_{i=1}^{3} d_i \int_0^\infty \{M_{2i}(\alpha)G_i(s, \alpha) + N_{2i}(\alpha)G_i'(s, \alpha), \}D(s)ds, \tag{B.1}$$

$$B_3(\alpha) = \frac{1}{\Delta(\alpha)} \sum_{i=1}^{3} d_i \int_0^\infty \{M_{3i}(\alpha)G_i(s, \alpha) + N_{3i}(\alpha)G_i'(s, \alpha), \}D(s), ds$$

where

$$G_i(s, \alpha) = \frac{2}{\pi} \frac{\gamma_i s^2}{s^2\gamma_i^2 + \alpha^2} J_0(bs),$$

$$G_i'(s, \alpha) = \frac{2}{\pi} \frac{\gamma_i s}{s^2\gamma_i^2 + \alpha^2} J_1(bs), \tag{B.2}$$

$$M_{1i}(\alpha) = m_i\{q_2(\alpha)r_3(\alpha) - q_3(\alpha)r_2(\alpha)\},$$

$$M_{2i}(\alpha) = m_i\{q_3(\alpha)r_1(\alpha) - q_1(\alpha)r_3(\alpha)\},$$

$$M_{3i}(\alpha) = m_i\{q_1(\alpha)r_2(\alpha) - q_2(\alpha)r_1(\alpha)\},$$

$$N_{1i}(\alpha) = \frac{(c_{12} - c_{11})a_i}{b}\{q_2(\alpha)r_3(\alpha) - q_3(\alpha)r_2(\alpha)\}$$

$$+\frac{f_i}{\gamma_i^2}\{r_2(\alpha)p_3(\alpha) - r_3(\alpha)p_2(\alpha)\} + \frac{n_i}{\gamma_i^2}\{p_2(\alpha)q_3(\alpha) - p_3(\alpha)q_2(\alpha)\},$$

(B.3)

$$N_{2i}(\alpha) = \frac{(c_{12} - c_{11})a_i}{b}\{q_3(\alpha)r_1(\alpha) - q_1(\alpha)r_3(\alpha)\}$$

$$+\frac{f_i}{\gamma_i^2}\{r_3(\alpha)p_1(\alpha) - r_1(\alpha)p_3(\alpha)\} + \frac{n_i}{\gamma_i^2}\{p_3(\alpha)q_1(\alpha) - p_1(\alpha)q_3(\alpha)\},$$

$$N_{3i}(\alpha) = \frac{(c_{12} - c_{11})a_i}{b}\{q_1(\alpha)r_2(\alpha) - q_2(\alpha)r_1(\alpha)\}$$

$$+\frac{f_i}{\gamma_i^2}\{r_1(\alpha)p_2(\alpha) - r_2(\alpha)p_1(\alpha)\} + \frac{n_i}{\gamma_i^2}\{p_1(\alpha)q_2(\alpha) - p_2(\alpha)q_1(\alpha)\},$$

$$(i = 1, 2, 3);$$

(B.4) $$\Delta(\alpha) = p_1(\alpha)\{q_2(\alpha)r_3(\alpha) - q_3(\alpha)r_2(\alpha)\} + p_2(\alpha)\{q_3(\alpha)r_1(\alpha)$$

$$- q_1(\alpha)r_3(\alpha)\} + p_3(\alpha)\{q_1(\alpha)r_2(\alpha) - q_2(\alpha)r_1(\alpha)\}$$

and

$$p_i(\alpha) = \alpha\gamma_i m_i I_0(\gamma_i'\alpha b) + \gamma_i^2 n_i I_1(\gamma_i'\alpha b),$$

(B.5) $$q_i(\alpha) = f_i I_1(\gamma_i'\alpha b), \qquad (i = 1, 2, 3);$$

$$r_i(\alpha) = n_i I_1(\gamma_i'\alpha b),$$

$$m_i = c_{11}a_i - c_{13} + e_{31}b_i,$$

(B.6)

$$n_i = e_{15}(a_i\gamma_i^2 + 1) + \epsilon_{11}b_i \qquad (i = 1, 2, 3).$$

Appendix C

The impermeable boundary condition becomes

$$\begin{aligned} &D_z(r,0) = 0 && (0 \le r < a), \\ &\phi(r,0) = 0 && (a \le r \le b). \end{aligned} \tag{C.1}$$

The boundary condition of Eq. (2.8) leads to Eq. (3.6). Making use of mixed boundary conditions of Eqs. (2.9) and (C.1), two simultaneous dual integral equations are obtained:

$$\begin{cases} \displaystyle\int_0^\infty \alpha F_{11} D_1(\alpha) J_0(\alpha r)\,d\alpha + \int_0^\infty \alpha F_{12} D_2(\alpha) J_0(\alpha r)\,d\alpha \\ \qquad\qquad \displaystyle -\sum_{j=1}^{3} \int_0^\infty \alpha g_j \gamma_j B_j(\alpha) I_0(\gamma_j' \alpha r)\,d\alpha = -\frac{\pi}{2}\sigma_\infty \quad (0 \le r < a) \\ \displaystyle\int_0^\infty D_1(\alpha) J_0(\alpha r)\,d\alpha = 0 \quad (a \le r \le b); \end{cases} \tag{C.2}$$

$$\begin{cases} \displaystyle\int_0^\infty \alpha F_{21} D_1(\alpha) J_0(\alpha r)\,d\alpha + \int_0^\infty \alpha F_{22} D_2(\alpha) J_0(\alpha r)\,d\alpha \\ \qquad\qquad \displaystyle -\sum_{j=1}^{3} \int_0^\infty \alpha h_j \gamma_j B_j(\alpha) I_0(\gamma_j' \alpha r)\,d\alpha = -\frac{\pi}{2} D^* \quad (0 \le r < a) \\ \displaystyle\int_0^\infty D_2(\alpha) J_0(\alpha r)\,d\alpha = 0 \quad (a \le r \le b), \end{cases} \tag{C.3}$$

where

$$\begin{aligned} D_1(\alpha) &= \frac{1}{\gamma_1} A_1(\alpha) + \frac{1}{\gamma_2} A_2(\alpha) + \frac{1}{\gamma_3} A_3(\alpha), \\ D_2(\alpha) &= \frac{b_1}{\gamma_1} A_1(\alpha) + \frac{b_2}{\gamma_2} A_2(\alpha) + \frac{b_3}{\gamma_3} A_3(\alpha); \end{aligned} \tag{C.4}$$

$$F_{11} = \sum_{j=1}^{3} g_j d_j, \quad F_{12} = \sum_{j=1}^{3} g_j l_j, \quad F_{21} = \sum_{j=1}^{3} h_j d_j, \quad F_{22} = \sum_{j=1}^{3} h_j l_j, \tag{C.5}$$

(C.6) $$l_1 = \gamma_1(f_2 - f_3), \quad l_2 = \gamma_2(f_3 - f_1), \quad l_3 = \gamma_3(f_1 - f_2)$$

(C.7) $$D^* = \begin{cases} D_\infty & \text{(Case I)}, \\ c_2\sigma_0 + e_3 E_\infty & \text{(Case II)}, \end{cases}$$

(C.8) $$c_2 = \frac{e_{33}(c_{11} + c_{12}) - 2c_{13}e_{31}}{(c_{11} + c_{12})c_{33} - 2c_{13}^2}, \quad e_3 = \frac{2e_{31}}{c_{11} + c_{12}} + \epsilon_{33};$$

(C.9)
$$B_1(\alpha) = \frac{1}{\Delta(\alpha)} \sum_{i=1}^{3} \int_0^\infty \{M_{1i}(\alpha)G_i(s,\alpha) + N_{1i}(\alpha)G_i'(s,\alpha)\}\{d_i D_1(s) + l_i D_2(s)\}ds,$$

$$B_2(\alpha) = \frac{1}{\Delta(\alpha)} \sum_{i=1}^{3} \int_0^\infty \{M_{2i}(\alpha)G_i(s,\alpha) + N_{2i}(\alpha)G_i'(s,\alpha)\}\{d_i D_1(s) + l_i D_2(s)\}ds,$$

$$B_3(\alpha) = \frac{1}{\Delta(\alpha)} \sum_{i=1}^{3} \int_0^\infty \{M_{3i}(\alpha)G_i(s,\alpha) + N_{3i}(\alpha)G_i'(s,\alpha)\}\{d_i D_1(s) + l_i D_2(s)\}ds.$$

The unknowns $D_1(\alpha)$ and $D_2(\alpha)$ can be found by the same method of approach as in the permeable case. The results are

(C.10)
$$D_1(\alpha) = -\frac{\sigma_\infty}{F_{11}} a^2 \int_0^1 \Phi_1(\xi)\sin(a\alpha\xi)d\xi,$$

$$D_2(\alpha) = -\frac{\sigma_\infty}{F_{12}} a^2 \int_0^1 \Phi_2(\xi)\sin(a\alpha\xi)d\xi.$$

The functions $\Phi_1(\xi)$ and $\Phi_2(\xi)$ in Eqs. (C.10) are the solutions of the following simultaneous Fredholm integral equations of the second kind:

$$\Phi_1(\xi) + \Phi_2(\xi) + \int_0^1 \Phi_1(\eta) K_{11}(\xi,\eta)d\eta + \int_0^1 \Phi_2(\eta) K_{12}(\xi,\eta)d\eta = \xi,$$

$$\text{(C.11)} \qquad \frac{F_{21}}{F_{11}}\Phi_1(\xi) + \frac{F_{22}}{F_{12}}\Phi_2(\xi).$$

$$+ \int_0^1 \Phi_1(\eta) K_{21}(\xi,\eta)d\eta + \int_0^1 \Phi_2(\eta) K_{22}(\xi,\eta)d\eta = \frac{D^*}{\sigma_\infty}\xi.$$

The kernels $K_{ij}(\xi,\eta)(i,j=1,2)$ are given by

$$K_{11}(\xi,\eta) = \frac{4}{\pi^2 F_{11}} \sum_{j=1}^{3} g_j \gamma_j^2 \int_0^\infty \frac{1}{\Delta(\alpha)} \sum_{i=1}^{3} d_i \gamma_i' \{\gamma_i' \alpha M_{ji}(\alpha) K_0(\gamma_i' \alpha b)$$

$$- N_{ji}(\alpha) K_1(\gamma_i' \alpha b)\} \sinh(\gamma_i' a\alpha\eta) \sinh(\gamma_j' a\alpha\xi) d\alpha,$$

$$K_{12}(\xi,\eta) = \frac{4}{\pi^2 F_{12}} \sum_{j=1}^{3} g_j \gamma_j^2 \int_0^\infty \frac{1}{\Delta(\alpha)} \sum_{i=1}^{3} l_i \gamma_i' \{\gamma_i' \alpha M_{ji}(\alpha) K_0(\gamma_i' \alpha b)$$

$$- N_{ji}(\alpha) K_1(\gamma_i' \alpha b)\} \sinh(\gamma_i' a\alpha\eta) \sinh(\gamma_j' a\alpha\xi) d\alpha,$$

$$\text{(C.12)}$$

$$K_{21}(\xi,\eta) = \frac{4}{\pi^2 F_{11}} \sum_{j=1}^{3} h_j \gamma_j^2 \int_0^\infty \frac{1}{\Delta(\alpha)} \sum_{i=1}^{3} d_i \gamma_i' \{\gamma_i' \alpha M_{ji}(\alpha) K_0(\gamma_i' \alpha b)$$

$$- N_{ji}(\alpha) K_1(\gamma_i' \alpha b)\} \sinh(\gamma_i' a\alpha\eta) \sinh(\gamma_j' a\alpha\xi) d\alpha,$$

$$K_{22}(\xi,\eta) = \frac{4}{\pi^2 F_{12}} \sum_{j=1}^{3} h_j \gamma_j^2 \int_0^\infty \frac{1}{\Delta(\alpha)} \sum_{i=1}^{3} l_i \gamma_i' \{\gamma_i' \alpha M_{ji}(\alpha) K_0(\gamma_i' \alpha b)$$

$$- N_{ji}(\alpha) K_1(\gamma_i' \alpha b)\} \sinh(\gamma_i' a\alpha\eta) \sinh(\gamma_j' a\alpha\xi) d\alpha.$$

The stress intensity factor k_1 and electric displacement intensity factor k_D for the impermeable crack are obtained as

$$\text{(C.13)} \qquad k_1 = \frac{2}{\pi}\sigma_\infty \sqrt{a}\{\Phi_1(1) + \Phi_2(1)\},$$

$$k_D = \frac{2}{\pi}\sigma_\infty\sqrt{a}\left\{\frac{F_{21}}{F_{11}}\Phi_1(1) + \frac{F_{22}}{F_{12}}\Phi_2(1)\right\}. \tag{C.14}$$

Using the field distribution in front of the crack border, the total potential energy release rate G and mechanical strain energy release rate G_M for the impermeable crack are

$$\begin{aligned} G = -\frac{\pi}{2(F_{11}F_{22} - F_{12}F_{21})^2}\Bigg[\Bigg\{(F_{11}F_{22} - F_{12}F_{21})\sum_{j=1}^{3}\frac{s_j}{\gamma_j} \\ -\sum_{j=1}^{3}h_j s_j \sum_{j=1}^{3}\frac{b_j s_j}{\gamma_j}\Bigg\} k_1^2 \\ +\Bigg\{\sum_{j=1}^{3}h_j t_j \sum_{j=1}^{3}\frac{b_j s_j}{\gamma_j} + \sum_{j=1}^{3}h_j s_j \sum_{j=1}^{3}\frac{b_j t_j}{\gamma_j} - (F_{11}F_{22} - F_{12}F_{21})\sum_{j=1}^{3}\frac{t_j}{\gamma_j}\Bigg\} k_1 k_D \\ -\left(\sum_{j=1}^{3}h_j t_j \sum_{j=1}^{3}\frac{b_j t_j}{\gamma_j}\right) k_D^2\Bigg], \end{aligned} \tag{C.15}$$

$$G_M = -\frac{\pi}{2(F_{11}F_{22} - F_{12}F_{21})}\left\{\left(\sum_{j=1}^{3}\frac{s_j}{\gamma_j}\right) k_1^2 - \left(\sum_{j=1}^{3}\frac{t_j}{\gamma_j}\right) k_1 k_D\right\}, \tag{C.16}$$

where

$$\begin{aligned} s_j &= d_j F_{22} - l_j F_{21}, \\ t_j &= d_j F_{12} - l_j F_{11}. \end{aligned} \tag{C.17}$$

The energy density factor are expressible in the forms

$$S = S_M + S_E, \tag{C.18}$$

where

$$S_M = \frac{1}{8(F_{11}F_{22} - F_{12}F_{21})^2}(\beta_1 k_1^2 + \beta_2 k_1 k_D + \beta_3 k_D^2), \tag{C.19}$$

$$S_E = \frac{1}{8(F_{11}F_{22} - F_{12}F_{21})^2}(\beta_4 k_1^2 + \beta_5 k_1 k_D + \beta_6 k_D^2), \tag{C.20}$$

(C.21)

$$\beta_1 = \sum_{j=1}^{3} m_j s_j R_j^c(\theta_1) \sum_{j=1}^{3} a_j s_j R_j^c(\theta_1) + 2\sum_{j=1}^{3} \frac{f_j s_j}{\gamma_j} R_j^s(\theta_1) \sum_{j=1}^{3} \frac{s_j(a_j\gamma_j^2+1)}{\gamma_j} R_j^s(\theta_1)$$
$$- \sum_{j=1}^{3} g_j s_j R_j^c(\theta_1) \sum_{j=1}^{3} s_j R_j^c(\theta_1),$$

$$\beta_2 = -\sum_{j=1}^{3} m_j t_j R_j^c(\theta_1) \sum_{j=1}^{3} a_j s_j R_j^c(\theta_1) - 2\sum_{j=1}^{3} \frac{f_j t_j}{\gamma_j} R_j^s(\theta_1) \sum_{j=1}^{3} \frac{s_j(a_j\gamma_j^2+1)}{\gamma_j} R_j^s(\theta_1)$$
$$+ \sum_{j=1}^{3} g_j t_j R_j^c(\theta_1) \sum_{j=1}^{3} s_j R_j^c(\theta_1) - \sum_{j=1}^{3} m_j s_j R_j^c(\theta_1) \sum_{j=1}^{3} a_j t_j R_j^c(\theta_1)$$
$$- 2\sum_{j=1}^{3} \frac{f_j s_j}{\gamma_j} R_j^s(\theta_1) \sum_{j=1}^{3} \frac{t_j(a_j\gamma_j^2+1)}{\gamma_j} R_j^s(\theta_1) + \sum_{j=1}^{3} g_j s_j R_j^c(\theta_1) \sum_{j=1}^{3} t_j R_j^c(\theta_1),$$

$$\beta_3 = \sum_{j=1}^{3} m_j t_j R_j^c(\theta_1) \sum_{j=1}^{3} a_j t_j R_j^c(\theta_1) + 2\sum_{j=1}^{3} \frac{f_j t_j}{\gamma_j} R_j^s(\theta_1) \sum_{j=1}^{3} \frac{t_j(a_j\gamma_j^2+1)}{\gamma_j} R_j^s(\theta_1)$$
$$- \sum_{j=1}^{3} g_j t_j R_j^c(\theta_1) \sum_{j=1}^{3} t_j R_j^c(\theta_1),$$

$$\beta_4 = \sum_{j=1}^{3} \frac{n_j}{\gamma_j} s_j R_j^s(\theta_1) \sum_{j=1}^{3} \frac{b_j s_j}{\gamma_j} R_j^s(\theta_1) - \sum_{j=1}^{3} h_j s_j R_j^c(\theta_1) \sum_{j=1}^{3} b_j s_j R_j^c(\theta_1),$$

$$\beta_5 = -\sum_{j=1}^{3} \frac{n_j}{\gamma_j} t_j R_j^s(\theta_1) \sum_{j=1}^{3} \frac{b_j s_j}{\gamma_j} R_j^s(\theta_1) + \sum_{j=1}^{3} h_j t_j R_j^c(\theta_1) \sum_{j=1}^{3} b_j s_j R_j^c(\theta_1)$$
$$- \sum_{j=1}^{3} \frac{n_j}{\gamma_j} s_j R_j^s(\theta_1) \sum_{j=1}^{3} \frac{b_j t_j}{\gamma_j} R_j^s(\theta_1) + \sum_{j=1}^{3} h_j s_j R_j^c(\theta_1) \sum_{j=1}^{3} b_j t_j R_j^c(\theta_1),$$

$$\beta_6 = \sum_{j=1}^{3} \frac{n_j}{\gamma_j} t_j R_j^s(\theta_1) \sum_{j=1}^{3} \frac{b_j t_j}{\gamma_j} R_j^s(\theta_1) - \sum_{j=1}^{3} h_j t_j R_j^c(\theta_1) \sum_{j=1}^{3} b_j t_j R_j^c(\theta_1).$$

References

1. Y. SHINDO, K. TANAKA, F. NARITA, *Singular stress and electric fields of a piezoelectric ceramic strip with a finite crack under longitudinal shear*, Acta Mech., **120**, 31–45, 1997.
2. Y. SHINDO, K. WATANABE, F. NARITA, *Electroelastic analysis of a piezoelectric ceramic strip with a central crack*, Int. J. Engng Sci. **38**, 1–19, 2000.
3. Y. E. PAK, *Crack extension force in a piezoelectric material*, ASME J. Appl. Mech., **57**, 647–653, 1990.
4. Y. SHINDO, E. OZAWA, J. P. NOWACKI, *Singular stress and electric fields of a cracked piezoelectric strip*, Int. J. Appl. Electromagnetics Mater., **1**, 77–87, 1990.
5. R.M. MCMEEKING, *Electrostrictive stresses near crack-like flaws*, J. Appl. Math. Phys., **40**, 615–627, 1989.
6. F. NARITA, Y. SHINDO, *Mode I crack growth rate for yield strip model of a narrow piezoelectric ceramic body*, Theoret. Appl. Fract. Mech., **36**, 73–85, 2001.
7. Y. SHINDO, H. MURAKAMI, K. HORIGUCHI, F. NARITA, *Evaluation of electric fracture properties of piezoelectric ceramics using the finite element and single-edge precracked-beam methods*, J. Am. Ceram. Soc., **85**, 1243–1248, 2002.
8. S. B. PARK, C. T. SUN, *Fracture criteria for piezoelectric ceramics*, J. Am. Ceram. Soc., **78**, 1475–1480, 1995.
9. Y. SHINDO, M. OKA, K. HORIGUCHI, *Analysis and testing of indentation fracture behavior of piezoelectric ceramics under an electric field*, ASME J. Eng. Mater. Tech., **123**, 293–300, 2001.
10. G. C. SIH, Mechanics of Fracture Initiation and Propagation, Kluwer Academic Publishers, The Netherlands 1991.
11. G. C. SIH, J. Z. ZUO, *Multiscale behavior of crack initiation and growth in piezoelectric ceramics*, Theoret. Appl. Fract. Mech., **34**, 123–141, 2000.

Received March 18, 2003.